Binder jetting of SS316L: a computational approach for droplet-powder interaction

Asif Ur Rehman
Department of Mechanical Engineering, Faculty of Engineering, Gazi University, Ankara, Türkiye, and ERMAKSAN, Bursa, Türkiye
Kashif Azher and Abid Ullah
Department of Mechanical Engineering, Faculty of Engineering, Gazi University, Ankara, Türkiye and
Additive Manufacturing Technologies Application and Research Center-EKTAM, Ankara, Türkiye
Celal Sami Tüfekci
Advanced Manufacturing Technologies Center of Excellence-URTEMM, Ankara, Türkiye, and
Metin Uymaz Salamci
Department of Mechanical Engineering, Faculty of Engineering, Gazi University, Ankara, Türkiye;
Additive Manufacturing Technologies Application and Research Center-EKTAM, Ankara, Türkiye and
Advanced Manufacturing Technologies Center of Excellence-URTEMM, Ankara, Türkiye

Abstract

Purpose – This study aims to describe the effects of capillary forces or action, viscosity, gravity and inertia via the computational fluid dynamics (CFD) analysis. The study also includes distribution of the binder droplet over the powder bed after interacting from different heights.

Design/methodology/approach – Additive manufacturing (AM) has revolutionized many industries. Binder jetting (BJT) is a powder-based AM method that enables the production of complex components for a wide range of applications. The pre-densification interaction of binder and powder is vital among various parameters that can affect the BJT performance. In this study, BJT process is studied for the binder interaction with the powder bed of SS316L. The effect of the droplet-powder distance is thoroughly analysed. Two different droplet heights are considered, namely, h1 (zero) and h2 (9.89 mm).

Findings – The capillary and inertial effects are predominant, as the distance affects these parameters significantly. The binder spreading and penetration depth onto the powder bed is influenced directly by the distance of the binder droplet. The former increases with an increase in latter. The binder distribution over the powder bed, whether uniform or not, is studied by the stream traces. The penetration depth of the binder was also observed along the cross-section of the powder bed through the same.

Originality/value – In this work, the authors have developed a more accurate representative discrete element method of the powder bed and CFD analysis of binder droplet spreading and penetration inside the powder bed using Flow-3D. Moreover, the importance of the splashing due to the binder's droplet height is observed. If splashing occurs, it will produce distortion in the powder, resulting in a void in the final part.

Keywords BJT printing, Binder, Powder bed, Droplet height, Capillary action, Inertial force, Flow pattern, Penetration depth

Paper type Research paper

1. Introduction

Additive manufacturing (AM) enables the production of complex forms and tailored designs with little preparatory time. Numerous advanced technological applications (Kok *et al.*, 2018) have grasped interest in AM Processes, such as aerospace industries (Guo and Leu, 2013), biomedicine (Tiwari *et al.*, 2015; Liu, 2012) and architecture (Ur Rehman and Sglavo, 2020; Ur Rehman and Sglavo, 2021). Binder jetting (BJT) has been categorized by ASTM/ISO as a powder based AM process (ISO/ASTM International, 2015). During the BJT process, the powder is spread on the build plate with a blade or roller. A printhead glides across

The current issue and full text archive of this journal is available on Emerald Insight at: **https://www.emerald.com/insight/1355-2546.htm**

Rapid Prototyping Journal

[DOI 10.1108/RPJ-08-2022-0264]

This project has received funding from the European Union's Horizon 2020 research and innovation programme under the Marie Skłodowska-Curie grant agreement No 764935 and 101034425.

Erratum: It has come to the attention of the Publisher that the article "Binder jetting of SS316L: a computational approach for droplet-powder interaction" by Asif Ur Rehman, Kashif Azher, Abid Ullah, Celal Sami Tüfekci and Metin Uymaz Salamci, published in *Rapid Prototyping Journal*, Vol. ahead-of-print, No. ahead-of-print, https://doi.org/10.1108/RPJ-08-2022-0264, included an error in Kashif Azher's affiliation. This error was introduced during the production process and the article has now been updated online. The affiliation has changed from Department of Mechanical Engineering, Faculty of Engineering, Gazi University, Ankara, Türkiye, and ERMAKSAN, Bursa, Türkiye to Department of Mechanical Engineering, Faculty of Engineering, Gazi University, Ankara, Türkiye and Additive Manufacturing Technologies Application and Research Center-EKTAM, Ankara, Türkiye. The publisher sincerely apologises for this error and for any confusion caused.

Received 16 August 2022
Revised 30 November 2022
13 March 2023
Accepted 27 March 2023

the powder bed, depositing binder droplets in a precise pattern (Allen and Sachs, 2000) following the powder deposition. The build platform is pushed down, and a spreading roller or blade distributes a fresh layer of powders when the layer is completed, and the process repeats itself over and over again until the part is complete. Unlike Powder Bed Fusion (PBF) technologies, BJT can work with almost any powder material. BJT has the broadest material selection of all AM processes (Utela *et al.*, 2008; Snelling *et al.*, 2017). There are various experimental techniques, such as using X-ray visualization of BJT process (Yamaguchi and Oya, 2022). However, the experimental techniques are expensive and cannot predict a significant distortion during manufacturing processes (Gibson *et al.*, 2015). The distortions created during the manufacturing process can lower the overall accuracy of the process in creating metallic parts (Gibson *et al.*, 2015). To overcome these limitations, computational methods are now being developed.

SS316L has been commonly used in a wide range of industrial applications considering its high strength, high oxidation and corrosion resistance and good heat resistance (Bautista *et al.*, 2003; Choi *et al.*, 2015; Simchi *et al.*, 2006). Generally, SS316L has been fabricated by BJT for applications such as electrochemical or bio-medical (Gokuldoss *et al.*, 2017) or depending upon the application; it can also be fabricated using BJT (Frykholm *et al.*, 2016) or LPBF (Hossain *et al.*, 2021; Lin *et al.*, 2020; Alharbi, 2022).

Computational fluid dynamics (CFD) can be applied to BJT in a various ways. A typical printer ejects millions of droplets onto the powder bed every second. CFD may help optimize the volume, forms, velocities and satellite formation of these droplets by taking into account the effects of nozzle geometries, temperature, bubble energy and material properties, including surface tension and viscosities (Pareekshith, 2020). Discrete element method (DEM) simulations can help research powder compaction under various roller configurations and particle size distributions (PSDs) (Wagner and Higgs, 2021). CFD has also been used to investigate droplet impact and subsequent binder absorption in the powder bed (Li *et al.*, 2022). It has been used to simulate a massive amount of spherical droplets impacting the powder bed in a CFD model (Pareekshith, 2020). This has been a valuable model for studying binder and powder interactions at the microscale, which will aid in optimization and scaling up the process (De Souza *et al.*, 2008). The CFD model has been used to define the binder infiltration, diffusion and coalescence in the powder bed (Miyanaji *et al.*, 2018). It has also been used to demonstrate how surface tension and capillary forces dominate and influence the flow of the binder within the powder bed (Wagner and Higgs, 2021; Nefzaoui and Skurtys, 2012). In a nutshell, CFD simulations have been used to optimize the build rate in a BJT process by providing a better knowledge of how different binder materials interact with powder (Pareekshith, 2020; Bai *et al.*, 2019).

Charles-Williams *et al.* (2011) conducted drop impact studies with minimal impact velocity on dry and pre-wetted powder and observed more spreading as compared to infiltration due to capillary action in granules production. Marston *et al.* (2013) studied the kinetics of liquid drop impact on powder using high-speed photography. According to their scaling analysis of experimental data, the observed spreading, rebound and splashing could be broadly described in three terms of the Weber number. The level-set and volume-of-fluid (VOF) methods have been used to follow the movements of the liquid droplet surface. There has been also a similarity in governing equations of both the methods (Jiang *et al.*, 2018; Van Mourik *et al.*, 2005; Afkhami and Bussmann, 2006).

According to the Weber and Ohnesorge numbers, the impact of a droplet on a solid surface can be categorized into four separate regions:

1 Inviscid impact-driven;
2 Capillarity-driven;
3 Extremely viscous capillarity-driven; and
4 Highly viscous impact-driven region (Schiaffino and Sonin, 1997).

The spreading velocity in each region can distinguish among these regions (Schiaffino and Sonin, 1997). Other experimental studies on the impact of droplets on the powder have also revealed that the same principle governs the impact (Lim *et al.*, 2009; van Dam and Le Clerc, 2004).

In this study, we have investigated the impact behaviour of the binder at different heights from the powder bed to optimize the conditions of the impact of the binder on the powder bed. The main driving forces have been pinpointed, e.g. inertial and capillary, the binder flow over the powder bed is revealed using stream traces. The representation of a powder bed using DEM help us to demonstrate variable particle size, which is very close to the actual condition of powder, along with a comparative analysis of our CFD model. Finally, the model is validated with the experimental findings.

2. Materials and methods

2.1 Powder bed modelling

The computation for the powder development and deposition process will be divided primarily into two steps: firstly, a variety of particles fall directly on the surface to create a powder stack; next, the blade/re-coater pushes across the surface at a defined velocity and particles advance into building chambers to formulate the layer.

The actual elastic contact force is measured using an interaction technique using the non-linear Hertz–Mindlin elastic equation [36], and the damping factor is theoretically used to recognize the dissipation of mechanical energy (Parteli and Pöschel, 2016; Cao, 2019; Tian *et al.*, 2020).

When such interacting particles overlap, the natural contact and damping forces in elastic materials are always in the perpendicular plane. Mass and Young's modulus are both equal, and the plane's relative stiffness is perpendicular. To account for the elastic contact force, no micro-slip method is used in the tangential path (Cleary and Sawley, 2002). Table 1 displays the D10, D50, D90 and nominal range of the SS316L (ERMAK-A11-S316L) PSD supplied by ERMAKSAN, Turkey. The PSD provided has been used to replicate the powder.

During the course of this study, the layer-by-layer deposition of SS316L stainless metal powder has been modelled using the

Table 1 SS316L particle size (μm) (Rehman *et al.*, 2021)

Nominal range	D10	D50	D90
15–45	19	30	46

Source: Table courtesy of Rehman *et al.* (2021)

Figure 1 (a) Discrete element modelling and (b) powder particle SEM (Rehman *et al.*, 2021)

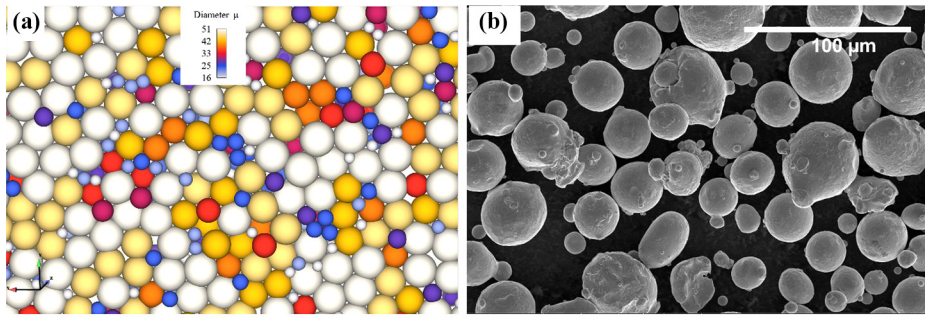

Source: Figure courtesy of Rehman *et al.* (2021)

DEM module from Flow Science, USA. Discrete microparticles were used to deposit a layer of powder rather than treating it as an equal-sized plate.

The powder particles are depicted in great detail in Figure 1. The particle sizes were observed to agree with D10, D50 and D90, and were known to match the experiment calculation. Displayed in Figure 1(a) is the particle produced by the model. The real powder particle may be roughly interpreted as spherical based on the SEM image in Figure 1(b).

2.2 Modelling of powder bed deposition process

The formation of SS316L metal powder was studied mainly using the theoretical model mentioned above. The layer of powder particles is 40-μm deep. The deposition procedure is schematically represented in Figure 2. The DEM simulation during powder bed deposition is shown in Figure 2(a). Figure 2(b) displays an isometric and top view of a 30-micron deposited layer. Figure 2(a) shows a 40-μm layer deposited in the DEM model. After retaining the voids within the block as the ones on the outer/free surface and after removing the ones on the outer/free surface, the layer of powder had a packing density of 65%. During the creation of the powder bed, Newton's Second Law can be used to find forces and movements that govern the DEM model. The normal and tangential forces that interact with spherical powder particles may be separated. The elastic normal contact force in the normal direction is calculated using a contact model using the non-linear elastic Hertz–Mindlin technique (Tian *et al.*, 2020). The following equations can be used to represent the elastic normal contact force:

$$F_C = Ku = \frac{4}{3}E^*\sqrt{R^*}u^{\frac{3}{2}} \tag{1}$$

Figure 2 (a) Powder bed deposition; (b) 30-micron deposited layer isometric and top view, and (c) side view (Rehman *et al.*, 2021)

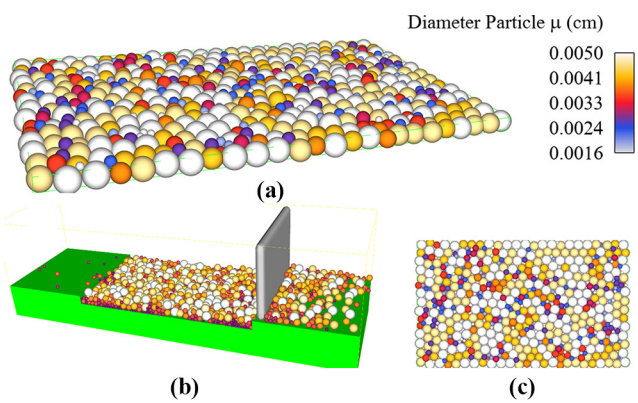

Source: Figure courtesy of Rehman *et al.* (2021)

2.3 Modeling of powder bed deposition process

This study examines the interaction of an ideal spherical droplet with the powder bed. Table 2 enlists the properties of the binder and some corresponding non-dimensional parameters. The properties given in Table 2 are derived from the formula from equations (1)–(5). In powder-based AM technologies, the size of powder particles generally lies in the micro-scale region. Herein, we assume that the powder bed consists of particles, as described in the previous section and represented in Figure 1. The interaction between the binder and powder involves changes in flow characteristics of the binder, from the impact to penetrating inside the powder bed. To understand the flow characteristics of the binder, some parameters are significant to be considered. Here, we have used the properties of the binder at room temperature and determined non-dimensional parameters. The high value of Froude and low value of Bond number show that the gravitational effect can be neglected on flow characteristics. Flow is laminar, as it corresponds to low Reynolds number and surface tension plays a significant role in spreading the binder, as indicated by the low value of the Ohnesorge number. The low Weber number also shows that the surface tension has a dominant effect compared to inertial forces during the flow. A detailed discussion about the behaviour of binder interaction with powder is presented in the result and discussion section. The corresponding impact velocities at different height is calculated by using the kinetic energy of the droplet (Nefzaoui and Skurtys, 2012):

$$\text{Reynolds}\left(Re = \frac{\rho VD}{\mu}\right) \tag{2}$$

$$\text{Weber}\left(We = \frac{\rho V^2 D}{\sigma}\right) \tag{3}$$

$$\text{Froude}\left(Fr = \frac{V^2}{gD}\right) \tag{4}$$

Table 2 Binder properties and non-dimensional parameters

Binder properties		h1		h2	
Density (kg/m^3)	997	*Fr*	171.429	*Fr*	571.429
Surface tension (N/m)	72×10^{-03}	*Bo*	0.017	*Bo*	0.017
Diameter (m)	3.50×10^{-05}	*Oh*	0.002	*Oh*	0.002
Viscosity (Pa.s)	8.8×10^{-04}	*We*	2.853	*We*	9.509
Velocity 1 (m/s)	0.242611	*Re*	9.620	*Re*	17.564
Velocity 2 (m/s)	0.420214	*Kd*	2.975	*Kd*	6.313

Source: Table courtesy of Rehman *et al.* (2021)

$$\text{Bond}\left(Bo = \frac{\rho g D^2}{\sigma}\right) \tag{5}$$

$$\text{Ohnesorge}\left(Oh = \frac{\mu}{\sqrt{\rho\sigma D}}\right) \tag{6}$$

2.4 Computational fluid dynamics modelling

A CFD framework was developed and implemented using particular subprocesses of the FLOW-3D CFD program. Flow Science, USA, Discrete Element Modelling (DEM) module was used in this CFD analysis. For simplicity, the research estimates several variables and generalizations, that is with Newtonian flow, the viscosity change brought on by the flow shearing is disregarded. It does not take much work to expand Newtonian flow to replicate non-Newtonian fluid (Tan, 2016). The incompressible, variable-density Navier–Stokes (NS) equations are used to model and solve such two-phase flow:

$$\nabla \cdot \boldsymbol{V} = 0 \tag{6}$$

$$\rho\frac{dV}{dt} + \rho(\boldsymbol{V}\cdot\nabla)\boldsymbol{V} = -\nabla P + \nabla\cdot\left[\mu(\nabla\boldsymbol{V}) + (\nabla\boldsymbol{V}^T)\right] + \sigma\delta mn \tag{7}$$

The last term represents the surface tension force and δ is dirac delta function; m and n are curvature and normal vectors of the interface, respectively (Tan, 2016).

2.5 Experimental setup of binder jet/binder dropping on powder bed

Parab *et al.* (2019) investigate the experimental setup shown in Figure 3 of SS316L powder particles interaction with binder, which is used to validate our developed simulation model. During the BJT process, a range of materials are studied with large spatial (2 μm) and temporal (5 μs) resolutions using a high-speed synchrotron hard X-ray imaging approach. The X-ray images indicate unique binder droplet behaviours, the interaction between the binder

Figure 4 (a) SS316L Powder distribution along the x and y plane and (b) the height of binder droplet along the *z*-axis

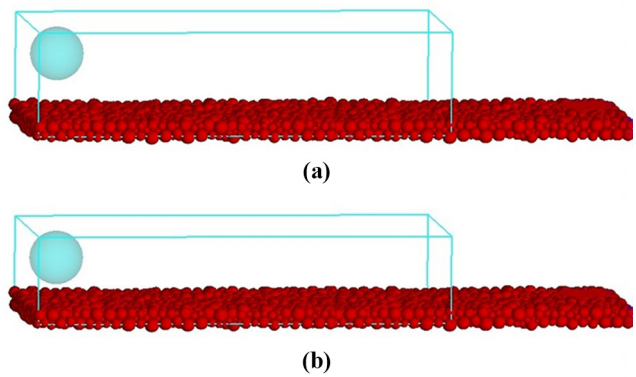

Source: Author's work

Figure 3 Schematic representation of experimental X-ray setup (Parab *et al.*, 2019)

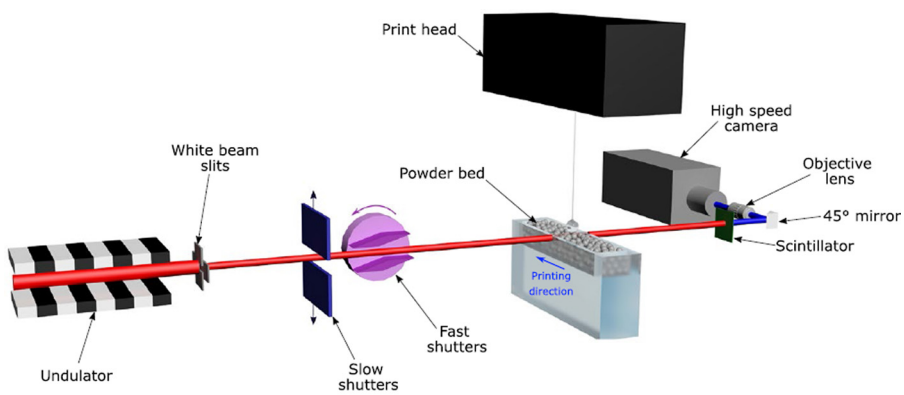

Source: Figure courtesy of Parab *et al.* (2019)

droplet and the powder bed and powder movement after the impact (Parab *et al.*, 2019).

3. Results and discussion

Initially, the droplet is located at the centre of the *x* and *y* plane and height "h1" and "h2" from the top of SS316L powder bed is varied from 0 to 9.89 mm, respectively. The droplet moves along the *z*-direction before interacting with powder. The schematic representation of the droplet and the powder bed is shown in Figure 4(a) and (b).

To investigate the effect of the difference in the height of a droplet from a SS316L powder bed, two different positions are considered. The simulation is carried out at h1 = 0 and h2 = 9.89 mm from the top of the powder bed to study the droplet's impact and penetration into powder. The corresponding Weber number is 2.853 and 9.509 for h1 and h2, respectively.

3.1 Binder dropping towards the powder from a small height

In Figure 5(a)–(d), the initial height "h1" is zero, and a slight wave can be observed coming from the top of the SS316L powder. The capillary wave formed when the droplet is at a small distance from the powder bed, and the capillary action is large as compared to inertial forces. Moreover, the binder faces resistance from powder at an early stage because of low wetting, which increases the capillary forces. During the early stages of the collision, the flow is inertial capillary and then falls into the capillary-viscous phase, similar to the change described by Das *et al.* (2012) and Tan (2016). The binder droplets form the surface over the powder bed once they settle, and there is no further movement. The surface tension and inertial force have a significant role in the impact of the binder droplet on the powder bed. The simulation time elapse is also shown in Figure 5, which is same as for all the figures.

The colour scheme at the right of the image shows the absorption of the binder in the powder bed. From Figure 6(a)–(d), the spreading of the binder at the powder bed is shown, and it can be observed that with an increase in time, the velocity of the binder droplet decreases, as it flows over the powder bed. In Figure 6(b), the two consecutive droplets can be distinguished based on their colour. In Figures 6(c) and (d), it can be observed that more binder penetrates near the impact area because the binder's lower inertial force and higher capillary action at the start of impact with powder favour the velocity increase. The capillary force action reduces with time and reduces the spreading of the binder throughout the powder bed length.

From Figure 7(a)–(d), the stream traces along with the binder can be observed. The arrows in Figure 7(c) and (d) show the flow direction of the binder over the powder bed. The increases in velocity after the impact with powder because of the reason mentioned earlier and then reduces. Moreover, the VF shows that most of the binder penetrates and spreads throughout the powder.

In Figure 8(a)–(b),the stream traces can be observed to first increase because of dominated capillary action and low inertial forces. In Figure 8(c)–(d), the velocity reduces with time, as most of the binder is absorbed inside the powder. The stream traces in Figure 8(d) show a nearby equilibrium state of the binder, as most of the stream traces diminish, as compared to Figure 8(b). It can also be observed from Figure 8(c) and (d) that stream traces move away from the centre of the powder bed. The spreading of the binder on the powder bed helps in

Figure 5 (a) Position of droplet before impact at height "h1"; (b) consecutive droplets with wave formation; (c) and (d) spreading of binder over the powder bed

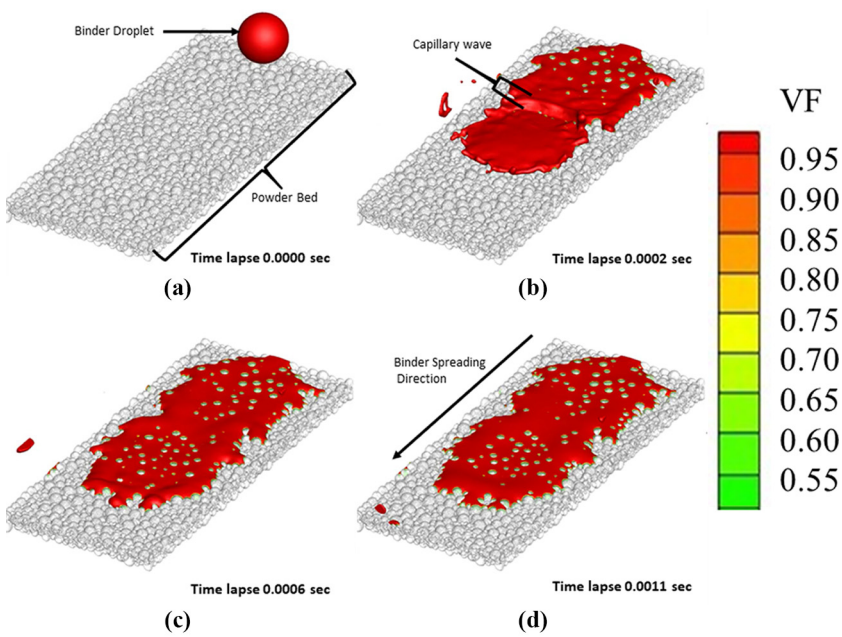

Note: VF = volume of fluid
Source: Author's work

Figure 6 (a) Position of droplet before impact; (b) two consecutive droplets with distinguish colours; (c) and (d) spreading of binder over the powder bed

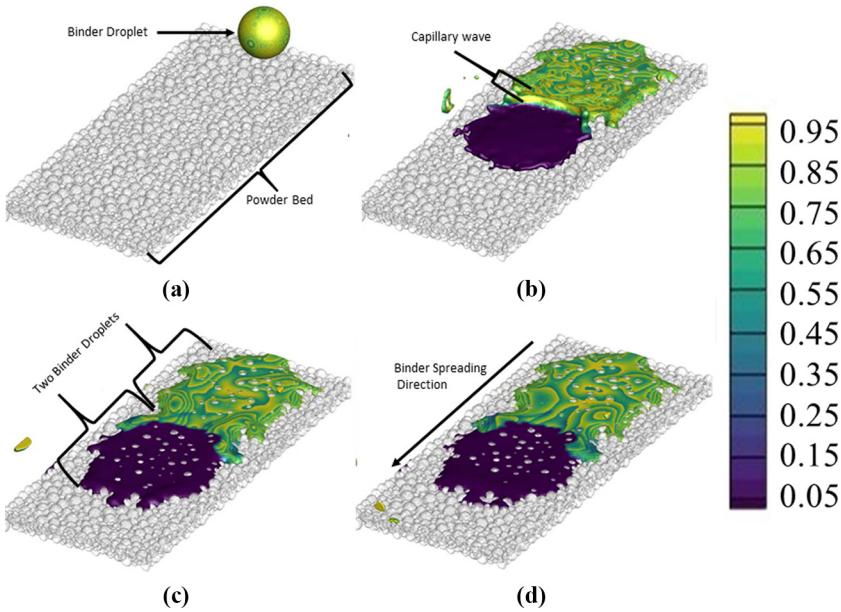

Note: The colour scheme at right shows the depth of the binder embedded into the powder bed
Source: Author's work

Figure 7 (a) Position of droplet before impact; (b) stream traces along with binder; (c) and (d) spreading of binder along with stream traces over the powder bed

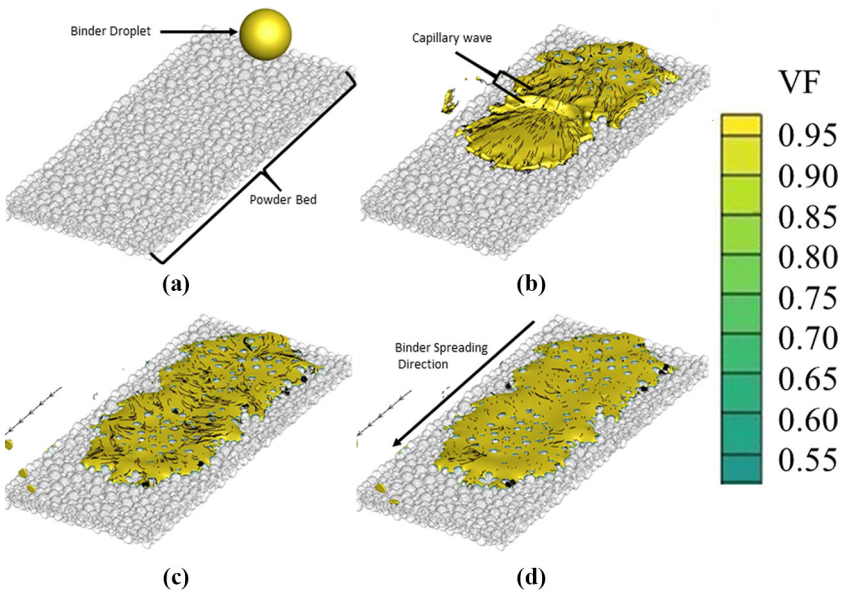

Source: Author's work

uniform distribution because lesser inertial force gives sufficient time for the binder to spread uniformly. The penetration depth is also shown along with the cross-section of the powder bed. The binder penetrated inside the depth is shown in yellow colour in Figure 8, and it is also labelled in the figure as "Binder penetrated in powder bed".

3.2 Binder dropping towards the powder from a large height

At droplet's height of h2 9.89 mm, the behaviour of the binder after impact with the SS316L powder is represented in Figure 9 (a)–(d). Compared to the height h1, which is zero, the inertial forces are more prevailing than the capillary forces from the start of the impact. In Figure 9(b), it can be observed that the

Figure 8 (a) Position of droplet before impact shown in the plane; (b) stream traces distribution after impact; (c) and (d) spreading of stream traces over the powder bed and equilibrium state

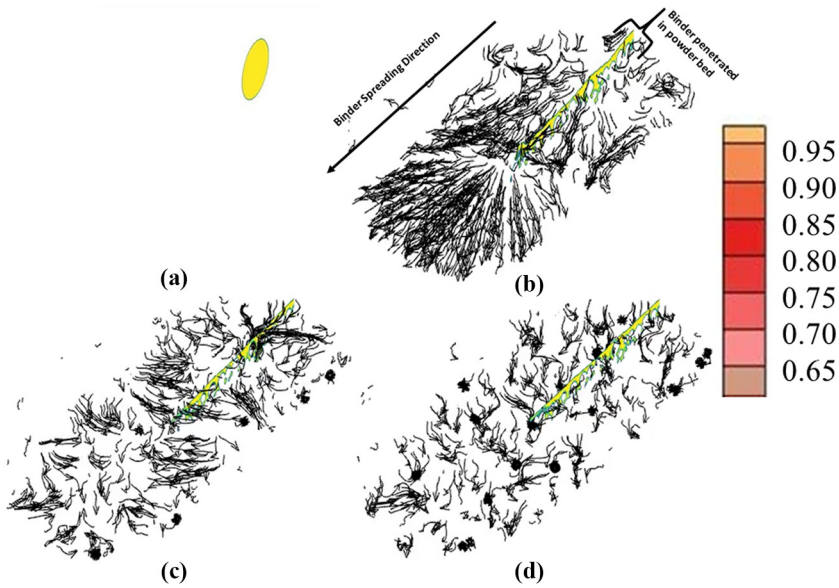

Source: Author's work

Figure 9 (a) Position of droplet before impact at large height; (b) consecutive droplets with wave formation; (c) and (d) spreading of binder over the powder bed

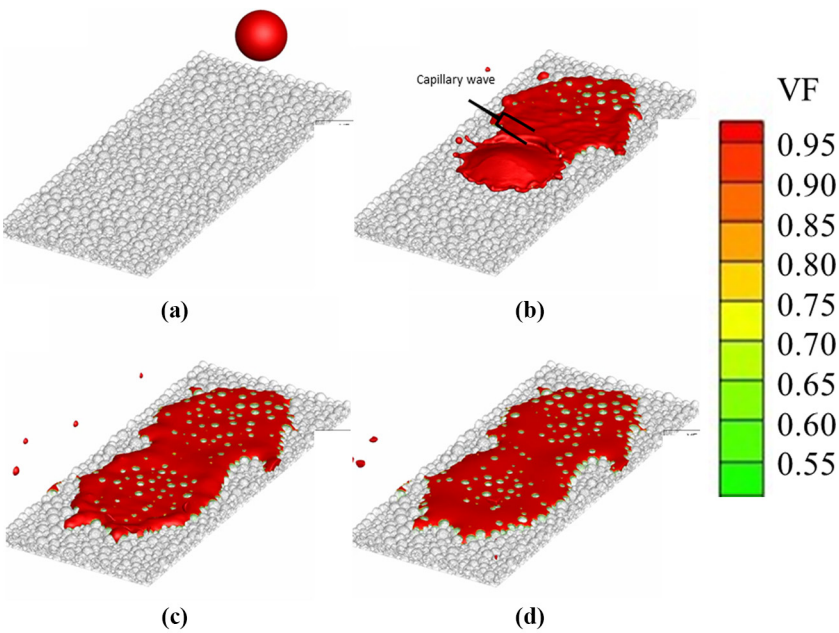

Source: Author's work

wave formed because of capillary action is small in comparison to Figure 5(b) for height h1. The small wave formation is because of more height; the droplet of the binder has more kinetic energy, which ultimately increases its inertial forces. It can also be observed from Figure 9(c) and (d) that the binder spread is significant over the powder bed because of more inertial forces. The binder droplet height effect the spreading and penetration of the binder inside the powder. As the height increases, the splashing or spreading increases, which also increases the spread of the binder over a wide area.

Similarly, in Figure 10(a)–(d), the binder spread and depth over the powder bed can be observed. In Figure 10(b), the two

Figure 10 (a) Position of droplet before impact at large height; (b) two consecutive droplets with distinguish colours; (c) and (d) spreading of binder over the powder bed

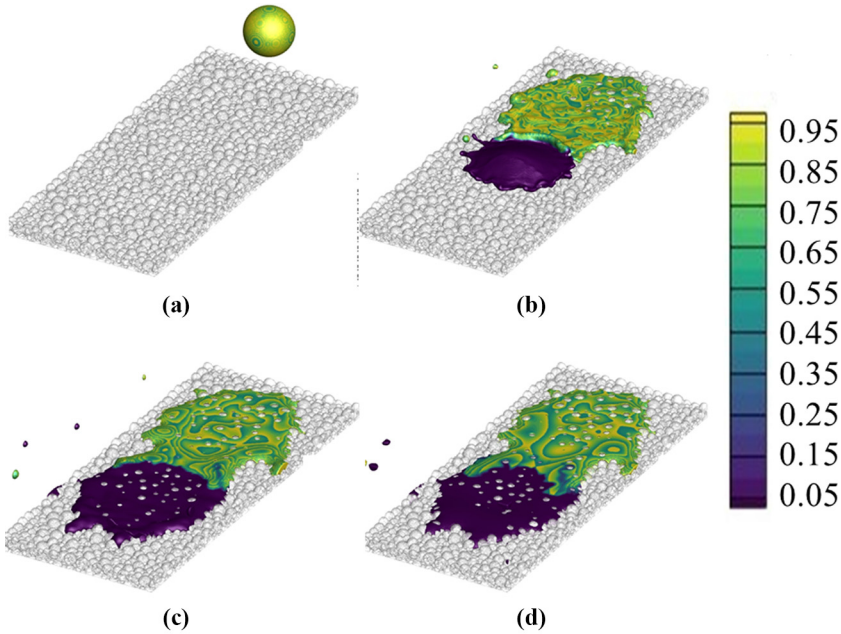

Note: The colour scheme at right shows the depth of the binder embedded into the powder bed
Source: Author's work

consecutive droplets can be distinguished based on their colour. From Figure 10(c) and (d), it can be observed that the penetration depth for the binder inside the powder bed increases more compared to Figure 6(c) and (d). The increase in binder spread and depth of penetration over the powder is because of more inertial forces as compared to capillary forces. As in this case, the height of the droplet is more, which increases its kinetic energy and has a significant effect on the distribution of the binder. The splashing and disturbance produced by the impact of the binder will be discussed in a later section.

In Figure 11(a)–(d), the stream traces can be observed similarly to Figure 8, increasing because of capillary action.

Figure 11 (a) Position of droplet before impact shown in the plane; (b) stream-traces distribution after impact; (c) and (d) spreading of stream traces over the powder bed and equilibrium state

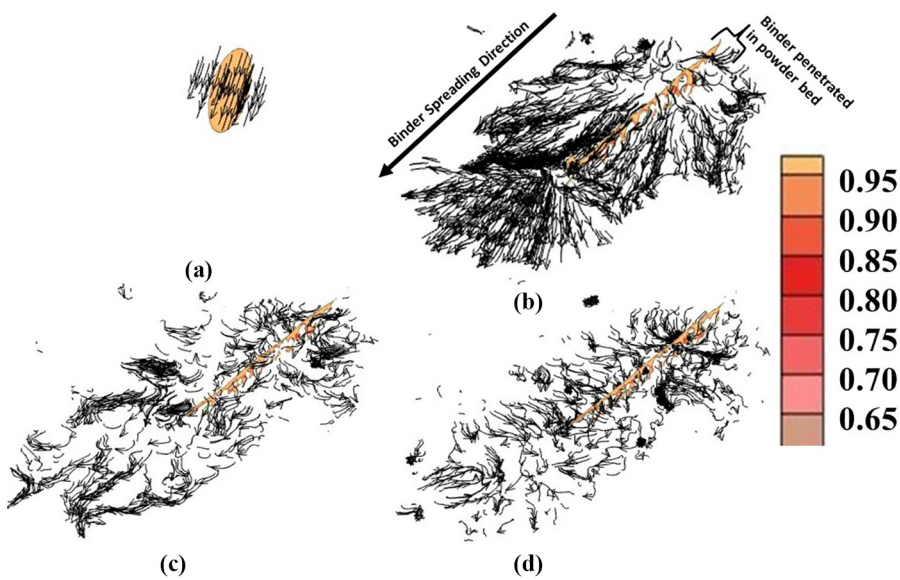

Source: Author's work

However, in Figure 9(b), the capillary wave is small because of dominant inertial forces. The velocity vector shows more inertial forces effect from the impact start and spreads throughout the powder bed. In Figure 11(c)–(d), similar to the previous Figure 8, the velocity reduces with time, as most of the binder is absorbed inside the powder. It can also be observed from Figure 11(c) and (d) that stream traces move away from the centre of the powder bed. However, the spreading of the binder on the powder bed is not very uniform, as the velocity vector does not have a specific direction. The binder distribution is also not uniform, although it covers a significant powder area. The stream traces in Figure 11(d) show a nearby equilibrium state of the binder, as most of the stream traces diminish compared to Figure 11(b).

The above discussion shows that penetration depth and binder spread over the powder bed is an essential considerations for BJT printing process. The droplet height increases the penetration depth, and the binder spreads over the powder. The thickness of powder bed layers in BJT printing is small, and if the penetration depth is not significant, it may result in insufficient hemming of layers. It can also reduce the strength of the end part in the direction of joining layers.

However, it should also be considered while selecting the height that the powder may undergo distortions with an increase in height and powder particles may segregate into each other, leading to dislocations or defects inside the final part. In addition, a term called splashing of the binder over the powder bed is widely used. The splashing parameter $k_d = We^{0.5}Re^{0.25}$ is defined as the parameter describing the spreading of a single drop into several tiny droplets upon impact (Nefzaoui and Skurtys, 2012). It was mainly observed for droplets having a splashing parameter greater than 120 [26]. No significant splashing occurs for two different heights used in our study, proving that the selected heights are suitable for printing of SS316L. However, in comparison, increasing the height increases the impact velocity, ultimately increasing the chances of splashing.

The experimental result shown here serves to compare two things that are splashing and binder penetration patterns in a powder bed. Similar to our model the splashing is observed in experimental work. So, the comparison for splashing is shown in Figure 12. The second observation is how the binder penetrates along the powder bed with time. As it can be observed from the X-ray and simulation results, the binder spread over the powder bed as it settles.

To validate our simulation effects on depth and splashing, we have also compared our findings with experimental findings. In Figure 12(a), high-speed hard X-ray imaging was used in the experiment by Parab *et al.* (2019). This technique can observe the impact of the binder droplet on the powder bed along the cross-section of the powder bed. The depth exhibited in this experiment indicates changes in the powder bed induced by powder particle movement and ejection triggered by the collision of the binder droplet and transfer of momentum between the droplet and powder particles. A large part of the momentum of the binder droplet was employed to distort the powder bed, with only 2% of the momentum contributing to powder particle ejection from the powder bed (Parab *et al.*, 2019). So the splashing is also very minimum in this experiment performed.

Figure 12(b) shows the penetration depth of the binder inside the powder bed along the plane. From Figure 12(b), it can be observed that the penetration depth of the binder is more near the area of impact and increases with an increase in time. This result can be correlated to the experimental findings shown in Figure 12(b), as the depth of binder penetration increases with the passage of time. The depth means here is the region which the binder cover after impact on the powder bed. So as time increases, the penetration of binder along the cross-section and the powder bed axis increases. Moreover, in our study, as mentioned above, no significant splashing occurs, as it creates significant disruptions in the powder bed. The experimental findings also reveal that minimum momentum is transferred from the binder impact to the powder bed, which distorts the powder bed, similar to our findings.

Figure 12 Interaction of the binder with the powder (a) X-ray analysis of binder with powder, the penetration depth shown by red mark (Parab *et al.*, 2019) and (b) CFD analysis of binder with powder, the penetration depth presented along the plane

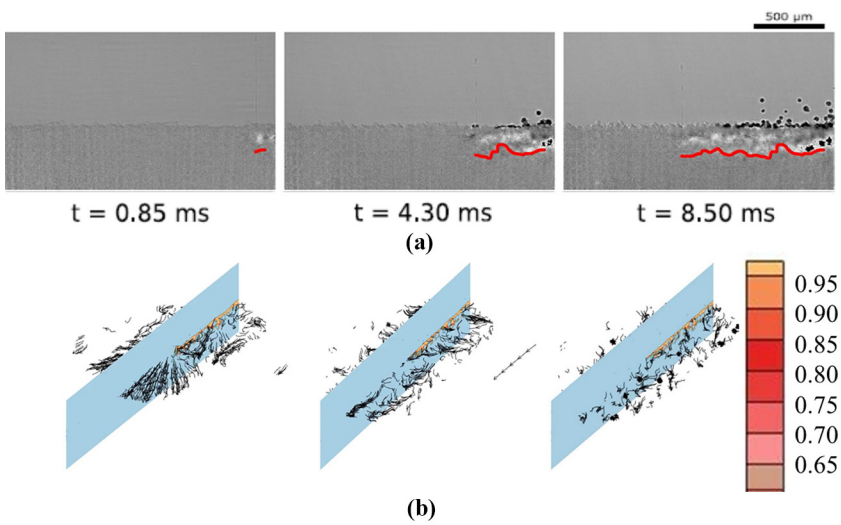

Sources: (a) Figure courtesy of Parab *et al.* (2019); (b) figure by Authors

4. Conclusion

This study developed a computational model for the BJT process by considering the VOF and discrete element modelling techniques. The impact between the binder and SS316L powder bed was observed. The height of the droplet was varied to investigate the effect of the binder on the powder bed. Moreover, the driving phenomena of inertia and capillary action of the binder were discussed. Furthermore, the penetration depth of the binder over the powder bed at various heights was observed. A comparative analysis of our study with the experimental analysis was performed. The findings from our simulation results had a strong correlation with the experimental results. On the basis of the current investigation, the following conclusions can be drawn:

- There is a significant effect of binder impact on the powder bed. Among various parameters that can affect the quality of BJT printing, selecting the correct height of the binder over the powder bed was vital. The height of the droplet can directly affect the penetration depth of the binder inside the powder. Increasing the height increases the penetration depth of the binder inside the powder.
- After the impact of the binder with the powder bed, the binder spreads based upon the principle of inertial and capillary forces. The inertial and capillary forces help the binder penetrate inside the powder. The inertial forces had a dominant role at the time of the impact. However, the capillary forces dominate when the height of the binder droplet is small as it can overcome inertial forces. The capillary forces reduce over time; therefore, the penetration depth is more under the area of impact.
- The capillary wave was formed over the powder bed where the capillary forces dominate compared to inertial forces. The stream traces observed during the binder and the powder interaction move across the length of the bed. The equilibrium position of the binder can be observed as the stream traces diminish over time.
- Increasing the velocity or binder height, increases the momentum, which induces the splashing. The excessive splashing distorts the powder bed and creates defects in the final part. In our study and other experimental findings, splashing was not very significant. The splashing was calculated using a splashing parameter whose value was less than 120 in our study.

This study provides an effective way to visualize different powder sizes on a single bed, which is near to the actual composition of the powder bed. Moreover, the effect of the droplet height is investigated, which could improve the quality of the final part and binder penetration depth inside the powder.

References

Afkhami, S. and Bussmann, M. (2006), "Drop impact simulation with a velocity-dependent contact angle".

Alharbi, N. (2022), "Shot peening of selective laser-melted SS316L with ultrasonic frequency", *Int J Adv Manuf Technol*, Vol. 119 Nos 3/4, pp. 2285-2299, doi: 10.1007/S00170-021-08398-0/FIGURES/11.

Allen, S.M. and Sachs, E.M. (2000), "Three-dimensional printing of metal parts for tooling and other applications", *Met Mater Int*, Vol. 6 No. 6, pp. 589-594, doi: 10.1007/BF03028104.

Bai, Y., Wall, C., Pham, H., Esker, A. and Williams, C.B. (2019), "Characterizing binder-powder interaction in binder jetting additive manufacturing via sessile drop goniometry", *J Manuf Sci Eng Trans ASME*, Vol. 141, p. 011005, doi: 10.1115/1.4041624/367169.

Bautista, A., Velasco, F. and Abenojar, J. (2003), "Oxidation resistance of sintered stainless steels: effect of yttria additions", *Corros Sci*, Vol. 45 No. 6, pp. 1343-1354, doi: 10.1016/S0010-938X(02)00217-2.

Cao, L. (2019), "Numerical simulation of the impact of laying powder on selective laser melting single-pass formation", *Int J Heat Mass Transf*, Vol. 141, pp. 1036-1048, doi: 10.1016/j.ijheatmasstransfer.2019.07.053.

Charles-Williams, H.R., Wengeler, R., Flore, K., Feise, H., Hounslow, M.J. and Salman, A.D. (2011), "Granule nucleation and growth: competing drop spreading and infiltration processes", *Powder Technol*, Vol. 206 Nos 1/2, pp. 63-71, doi: 10.1016/j.powtec.2010.06.013.

Choi, J.P., Lee, G.Y., Song, J.I., Lee, W.S. and Lee, J.S. (2015), "Sintering behavior of 316L stainless steel micro–nanopowder compact fabricated by powder injection molding", *Powder Technol*, Vol. 279, pp. 196-202, doi: 10.1016/J.POWTEC.2015.04.014.

Cleary, P.W. and Sawley, M.L. (2002), "DEM modelling of industrial granular flows: 3D case studies and the effect of particle shape on hopper discharge", *Appl Math Model*, Vol. 26 No. 2, pp. 89-111, doi: 10.1016/S0307-904X(01)00050-6.

Das, S., Waghmare, P.R. and Mitra, S.K. (2012), "Early regimes of capillary filling", *Physical Review E*, Vol. 86 No. 6, p. 067301, doi: 10.1103/PHYSREVE.86.067301/FIGURES/3/MEDIUM.

De Souza, E.J., Gao, L., McCarthy, T.J., Arzt, E. and Crosby, A.J. (2008), "Effect of contact angle hysteresis on the measurement of capillary forces", *Langmuir*, Vol. 24 No. 4, pp. 1391-1396, doi: 10.1021/LA702188T/ASSET/IMAGES/MEDIUM/LA702188TN00001.GIF.

Frykholm, R., Takeda, Y., Andersson, B.G. and Carlstrom, R. (2016), "Solid state sintered 3-D printing component by using inkjet (binder) method", *Journal of the Japan Society of Powder and Powder Metallurgy*, Vol. 63 No. 7, pp. 421-426, doi: 10.2497/jjspm.63.421.

Gibson, I., Rosen, D. and Stucker, B. (2015), *Additive Manufacturing Technologies*, Springer New York, NY.

Gokuldoss, P.K., Kolla, S. and Eckert, J. (2017), "Additive manufacturing processes: selective laser melting, electron beam melting and binder jetting-selection guidelines", *Materials*, Vol. 10 No. 6, p. 672, doi: 10.3390/MA10060672.

Guo, N. and Leu, M.C. (2013), "Additive manufacturing: technology, applications and research needs", *Front Mech Eng*, Vol. 8 No. 3, pp. 215-243, doi: 10.1007/s11465-013-0248-8.

Hossain, U., Ghouse, S., Nai, K. and Jeffers, J.R.T. (2021), "Mechanical and morphological properties of additively manufactured SS316L and Ti6Al4V micro-struts as a function of build angle", *Addit Manuf*, Vol. 46, p. 102050, doi: 10.1016/J.ADDMA.2021.102050.

ISO/ASTM International (2015), "ISO/ASTM 52900 – Additive manufacturing – General principles – terminology", pp. 1-26.

Jiang, M., Zhou, B. and Wang, X. (2018), "Comparisons and validations of contact angle models", *Int J Hydrogen Energy*, Vol. 43 No. 12, pp. 6364-6378, doi: 10.1016/J.IJHYDENE.2018.02.016.

Kok, Y., Tan, X.P., Wang, P., Nai, M.L.S., Loh, N.H., Liu, E. and Tor, S.B. (2018), "Anisotropy and heterogeneity of microstructure and mechanical properties in metal additive manufacturing: a critical review", *Mater Des*, Vol. 139, pp. 565-586, doi: 10.1016/j.matdes.2017.11.021.

Li, X.P., Wang, Y.E., Ahmed, A., Wei, Q.H., Guo, Y., Zhang, K. and Shi, Y.K. (2022), "The study of biological glue droplet impact behavior of bioceramic powders applied in 3D printing of bone scaffolds", *Applied Sciences*, Vol. 12 No. 4, p. 1898, doi: 10.3390/APP12041898.

Lim, T., Han, S., Chung, J., Chung, J.T., Ko, S. and Grigoropoulos, C.P. (2009), "Experimental study on spreading and evaporation of inkjet printed pico-liter droplet on a heated substrate", *Int J Heat Mass Transf*, Vol. 52 Nos 1/2, pp. 431-441, doi: 10.1016/J.IJHEATMASSTRANSFER.2008.05.028.

Lin, P.Y., Shen, F.C., Wu, K.T., Hwang, S.J. and Lee, H.H. (2020), "Process optimization for directed energy deposition of SS316L components", *Int J Adv Manuf Technol*, Vol. 111 Nos 5/6, pp. 1387-1400, doi: 10.1007/S00170-020-06113-Z/FIGURES/16.

Liu, F.H. (2012), "Synthesis of bioceramic scaffolds for bone tissue engineering by rapid prototyping technique", *J Sol-Gel Sci Technol*, Vol. 64 No. 3, pp. 704-710, doi: 10.1007/s10971-012-2905-5.

Marston, J.O., Sprittles, J.E., Zhu, Y., Li, E.Q., Vakarelski, I.U. and Thoroddsen, S.T. (2013), "Drop spreading and penetration into pre-wetted powders", *Powder Technol*, Vol. 239, pp. 128-136, doi: 10.1016/j.powtec.2013.01.062.

Miyanaji, H., Zhang, S. and Yang, L. (2018), "A new physics-based model for equilibrium saturation determination in binder jetting additive manufacturing process", *Int J Mach Tools Manuf*, Vol. 124, pp. 1-11, doi: 10.1016/J.IJMACHTOOLS.2017.09.001.

Nefzaoui, E. and Skurtys, O. (2012), "Impact of a liquid drop on a granular medium: inertia, viscosity and surface tension effects on the drop deformation", *Exp Therm Fluid Sci*, Vol. 41, pp. 43-50, doi: 10.1016/j.expthermflusci.2012.03.007.

Parab, N.D., Barnes, J.E., Zhao, C., Cunningham, R.W., Fezzaa, K., Rollett, A.D. and Sun, T. (2019), "Real time observation of binder jetting printing process using high-speed X-ray imaging", *Sci Rep*, Vol. 9 No. 1, pp. 1-10, doi: 10.1038/s41598-019-38862-7.

Pareekshith, A.M. (2020), "CFD simulation for metal additive manufacturing: applications in laser- and sinterbased processes", Met. Addit. Manuf, pp. 151-158.

Parteli, E.J.R. and Pöschel, T. (2016), "Particle-based simulation of powder application in additive manufacturing", *Powder Technol*, Vol. 288, pp. 96-102, doi: 10.1016/j.powtec.2015.10.035.

Rehman, A.U., Pitir, F. and Salamci, M.U. (2021), "Full-field mapping and flow quantification of melt Pool dynamics in laser powder bed fusion of SS316L", *Materials (Basel)*, Vol. 14 No. 21, pp. 16-19, doi: 10.3390/ma14216264.

Schiaffino, S. and Sonin, A.A. (1997), "Molten droplet deposition and solidification at low weber numbers", *Phys Fluids*, Vol. 9 No. 11, pp. 3172-3187, doi: 10.1063/1.869434.

Simchi, A., Rota, A. and Imgrund, P. (2006), "An investigation on the sintering behavior of 316L and 17-4PH stainless steel powders for graded composites", *Mater Sci Eng A*, Vol. 424 Nos 1/2, pp. 282-289, doi: 10.1016/J.MSEA.2006.03.032.

Snelling, D.A., Christopher, Williams, B., Carlos, Suchicital, T.A., Druschitz, A.P., Williams, C.B. and Suchicital, C.T.A. (2017), "Binder jetting advanced ceramics for metal-ceramic composite structures", *The International Journal of Advanced Manufacturing Technology*, Vol. 92 Nos 1/4, pp. 531-545, doi: 10.1007/S00170-017-0139-Y.

Tan, H. (2016), "Three-dimensional simulation of micrometer-sized droplet impact and penetration into the powder bed", *Chem Eng Sci*, Vol. 153, pp. 93-107, doi: 10.1016/J.CES.2016.07.015.

Tian, Y., Yang, L., Zhao, D., Huang, Y. and Pan, J. (2020), "Numerical analysis of powder bed generation and single track forming for selective laser melting of SS316L stainless steel", *J Manuf Process*, Vol. 58, pp. 964-974, doi: 10.1016/J.JMAPRO.2020.09.002.

Tiwari, S.K., Pande, S., Agrawal, S. and Bobade, S.M. (2015), "Selection of selective laser sintering materials for different applications", *Rapid Prototyping Journal*, Vol. 21 No. 6, pp. 630-648, doi: 10.1108/RPJ-03-2013-0027.

Ur Rehman, A. and Sglavo, V.M. (2020), "3D printing of geopolymer-based concrete for building applications", *Rapid Prototyp J*, Vol. 26 No. 10, pp. 1783-1788, doi: 10.1108/RPJ-09-2019-0244.

Ur Rehman, A. and Sglavo, V.M. (2021), "3D printing of Portland cement-containing bodies", *Rapid Prototyp J*, Vol. 28 No. 2, pp. 197-203, doi: 10.1108/RPJ-08-2020-0195.

Utela, B., Storti, D., Anderson, R. and Ganter, M. (2008), "A review of process development steps for new material systems in three dimensional printing (3DP)", *J Manuf Process*, Vol. 10 No. 2, pp. 96-104, doi: 10.1016/J.JMAPRO.2009.03.002.

van Dam, D.B. and Le Clerc, C. (2004), "Experimental study of the impact of an ink-jet printed droplet on a solid substrate", *Physics of Fluids*, Vol. 16 No. 9, p. 3403, doi: 10.1063/1.1773551.

Van Mourik, S., Veldman, A.E.P. and Dreyer, M.E. (2005), "Simulation of capillary flow with a dynamic contact angle", *Microgravity - Sci Technol*, Vol. 17 No. 3, pp. 87-93, doi: 10.1007/BF02872093.

Wagner, J.J. and Higgs, C.F. (2021), "Computation of hydrodynamic and capillary phenomena in binder jet three-dimensional printing", *Journal of Tribology*, Vol. 143 No. 5, pp. 1-15, doi: 10.1115/1.4050942.

Yamaguchi, D. and Oya, N. (2022), "In situ visualization of aluminum sintering for binder jetting by X-ray transmission", *The International Journal of Advanced Manufacturing Technology*, Vol. 121 Nos 5/6, pp. 3965-3975, doi: 10.1007/S00170-022-09601-6.

Corresponding authors

Asif Ur Rehman can be contacted at: asyf.rehman@gmail.com and **Kashif Azhar** can be contacted at: kashifazher92@gmail.com